A&A 434, 585–592 (2005)
DOI: 10.1051/0004-6361:20041086

Astronomy & Astrophysics

Star formation in Sandqvist 187 and 188⋆,⋆⋆

M. Nielbock and R. Chini

Astronomisches Institut der Ruhr-Universität Bochum, Universitätsstraße 150, 44780 Bochum, Germany
e-mail: [nielbock;chini]@astro.rub.de

Received 14 April 2004 / Accepted 17 December 2004

Abstract. We present 1.2 mm continuum data of the filamentary dark cloud Sandqvist 187/188 – also known as the Norma cloud – taken with SIMBA (SEST Imaging Bolometer Array). The data are complemented by measurements from the *2MASS*, *MSX* and *IRAS* surveys. The extended 1.2 mm emission traces the optical dark cloud down to a visual extinction of A_V = 3.7 mag. We derive a mean column density of $N(H_2) = 1.4 \times 10^{22}$ cm^{-2}, equivalent to a visual extinction of $A_V = 7.6$ mag and a total mass of the cloud of 340 $M_\odot$. We also find six compact millimetre sources, labelled MMS 1 to 6, five of which coincide with known stellar objects. MMS 6, however, only has a very weak *MSX* counterpart at 14.56 μm and an absorption feature at 8.28 μm consistent with a visual extinction of $A_V > 145$ mag. Dust temperatures, luminosities and gas masses for all compact millimetre sources are given. In an effort to further constrain the uncertain distance to Sandqvist 187/188, we analyse its stellar content based on *2MASS* colours and find an improved lower limit of 440 ± 50 pc.

Key words. ISM: clouds – dust, extinction – ISM: individual objects: Sandqvist 187 – ISM: individual objects: Sandqvist 188 – stars: pre-main sequence

1. Introduction

Low-mass stars are mostly formed in dark clouds that are silhouetted against the background of field stars. These clouds have a large variety of different shapes, among them being globules (e.g. Bourke et al. 1995) and filaments (e.g. Schneider & Elmegreen 1979).

Sandqvist 187 and 188 (Sa 187/188) were first listed and categorised as dark clouds by Sandqvist (1977). Their approximate position is α(J2000) = 16^h34^m, δ(J2000) = −45°00′ (G338.67+1.88) in the Norma star-forming region. On optical DSS images, they clearly stand out as an interconnected cloud filament in front of numerous background stars. With a typical width of 3′–4′ and a length of 40′ they comprise a combined area of 150□′. Four *IRAS* point sources have been found inside the FDC. Cloud distance estimates lie between 150 pc (Gregorio Hetem et al. 1988) and 700 pc (Graham & Frogel 1985).

So far, only Alvarez et al. (1986) have studied the global properties of the Sa 187/188 cloud by means of CO molecular spectroscopy mapping at a frequency of 115 GHz and at a low resolution of 8.′8 (HPBW). Assuming a distance of 700 pc, the authors estimated the total mass of the cloud to be 500 $M_\odot$ with a column density of $N(H_2) = 1.4 \times 10^{21}$ cm^{-2}.

Many investigations concentrate on a small region in the vicinity of two Herbig-Haro objects on the western edge of Sa 187, HH 56 and HH 57 and their associated stellar sources. Among them is V346 Nor, a FU Ori star (e.g. Graham & Frogel 1985; Prusti et al. 1993; Reipurth et al. 1997; Ábrahám et al. 2004) confirming that Sa 187/188 is a site of active star formation. Moreira et al. (2000) found a second star-forming core towards the *IRAS* point source IRAS 16295-4452 by millimetre molecular spectroscopy in CO and CS roughly 5′ east of the HH 56/57 region. They categorised the *IRAS* source as a YSO of Class I.

Here we report on the first large-scale 1.2 mm continuum observations of Sa 187/188. We derive parameters of the cloud ISM and include infrared measurements from the *2MASS*, *MSX* and *IRAS* projects in our analysis. The physical properties of six newly detected embedded compact millimetre continuum sources are listed as well. Finally, we discuss the possible star formation history of Sa 187/188 with respect to the filamentary nature of the cloud.

2. Observations and data reduction

The observations with the SEST Millimetre Bolometer Array (SIMBA) were carried out between July 31st and August 6th, 2003. SIMBA (Nyman et al. 2001) consists of 37 horn antennae aligned in a hexagonal configuration, each of them having a half-power beam width (HPBW) of roughly 24″ at a frequency of 250 GHz (λ = 1.2 mm). The full width at half power (FWHP) of the continuum filter transmission is 90 GHz. The SEST (Swedish ESO Submillimetre Telescope) has a 15 m aluminium coated dish optimised for submillimetre (submm) wavelengths. It is located at the ESO site of La Silla, Chile,

⋆ Based on observations collected at the European Southern Observatory, La Silla, Chile (71.C-0069).

⋆⋆ Appendices A, B and C are only available in electronic form at http://www.edpsciences.org

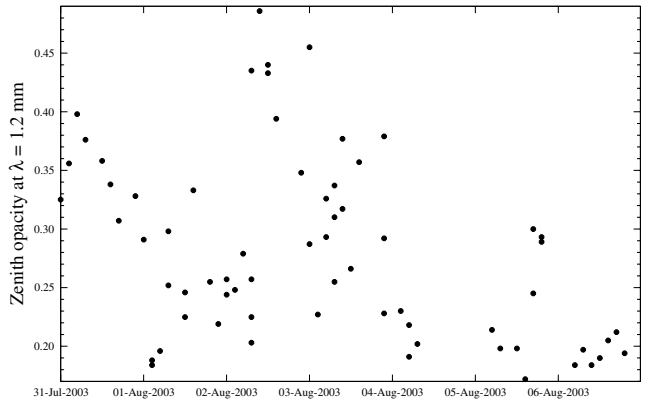

Fig. 1. Measured zenith opacities τ_0 at $\lambda = 1.2$ mm throughout the observing run.

at an altitude of about 2400 m and was de-commissioned in August 2003.

We used the fast-scanning mode (Reichertz et al. 2001) with a scanning speed of $80'' \, s^{-1}$. Altogether, the data comprise 90 maps which are partially overlapping in order to improve the spatial coverage and reduce the residual noise. Additional maps of Neptune and Uranus were obtained for calibration purposes yielding a conversion factor of 50.6 ± 4.1 mJy count^{-1}. The atmospheric opacity at $\lambda = 1.2$ mm was derived from frequent skydips in order to correct for the atmospheric extinction during the data reduction process. The zenith optical depth varied between 0.17 and 0.45 (Fig. 1). For most of the time, the variations were slow enough to be accounted for in the data reduction to an accuracy of better than ±0.05. The SEST was equipped with a pointing model which was accurate to $\pm 2\farcs5$ (rms). Short term deviations were checked and corrected with frequent pointings on strong continuum point sources (Mars, Uranus, Neptune, Cen A, QSO 1757-240).

We reduced the data with an improved successor of MOPSI called MOPSIC[1] in an iterative way. This includes de-spiking, baseline fitting, deconvolution of the bolometer passband, correction for the atmospheric opacity and the gain-elevation influence and – most importantly – the filtering of the correlated sky noise (SIMBA Manual 2003). For a more detailed description of the procedure, we refer to the paper of Chini et al. (2003).

The residual noise in the final map varies locally depending on the observational coverage. The noise level in the western part of the map is ∼6−7 mJy/beam and increases to ∼8−9 mJy/beam in the vicinity of IRAS 16311-4457. In the easternmost part of the map, the noise level is ∼11−12 mJy/beam.

The photometry of the compact millimetre sources was carried out by integrating over 2-dimensional Gaussian fits to the sources. This procedure allows us to measure the flux from the source alone and reject the background emission. The error of the photometry was derived from the remaining local noise after subtracting the Gaussian: we determined the area the Gaussian covers for flux values above the 1σ level and calculated the number of beams N this corresponds to. The photometric error is:

$$\Delta S = \sqrt{N} \times \sigma \cdot \quad (1)$$

In the case of MMS 3 and MMS 4, distinct millimetre sources are evident from the maps, although they cannot be separated in the fitting procedure. Here we fitted a combined Gaussian and analysed their mutual properties.

The *MSX* data were retrieved from the IPAC Infrared Science Archive. We carried out new photometry in all 4 available filter bands (A: 8.28 μm, C: 12.13 μm, D: 14.65 μm, E: 21.34 μm) in a similar manner as described for the millimetre data. The images were flux calibrated[2] (Egan et al. 1999) but no colour corrections were applied because of the sufficiently high temperatures of the various sources. We checked the resolution with a set of known bright point sources (α Cyg, λ Sco, α Sct) and found a mean PSF size of $21\farcs3$ with a standard deviation of $0\farcs3$ for all filter bands.

3. Results

In this section, we present the SIMBA 1.2 mm map of the Sa 187/188 region and discuss the extended mm emission as well as the protostellar content by comparing our data with those from the *MSX* and *2MASS* data archives. For comparison, we will use the widely adopted distance of 700 pc, which is compatible with our lower limit of 440 pc (see Appendix B).

3.1. Extended millimetre emission

Figure 2 shows our SIMBA mm map of the Sa 187/188 region. The distribution of the extended mm emission follows very well the absorption structure visible on DSS images. The total flux density of the extended emission above 3σ rms amounts to 8.7 Jy without the compact sources. With an assumed dust temperature of $T_{\rm dust} = 20$ K, a dust mass absorption coefficient of $\kappa_{1.2} = 0.03$ cm^2 g^{-1}, typical of unprocessed ISM (Krügel & Siebenmorgen 1994), and a gas-to-dust ratio of 140, we find a total mass of $M(H_2) = 340 \, M_\odot$; here, we assume a mean molecular weight of 4×10^{-24} g per H_2 molecule which includes 1 He atom for every five H_2 molecules. This mass amounts to 70% of the value Alvarez et al. (1986) derived from their ^{13}CO observations; this is compatible with the tendency of ^{13}CO measurements to be more sensitive to low density gas than our continuum observations. Altogether, we estimate a mean gas column density of $N(H_2) = 1.4 \times 10^{22}$ cm^{-2} which is equivalent to a visual extinction of $A_V = 7.6$ mag using the transformation of Bohlin et al. (1978) and a normal ratio of total to selective extinction of 3.09.

The residual noise in the SIMBA map ranges from 6 to 11 mJy beam^{-1} (1σ rms) corresponding to a minimum detectable column density of $N(H_2) = 7.0 \times 10^{21}$ cm^{-2} (3σ) in the western and central region of the mm map. In other words, our observations can only detect dust that produces a visual

[1] Created and constantly updated by Robert W. Zylka, IRAM, Grenoble, France.

[2] `irsa.ipac.caltech.edu/applications/MSX/imageDescriptions.htm`

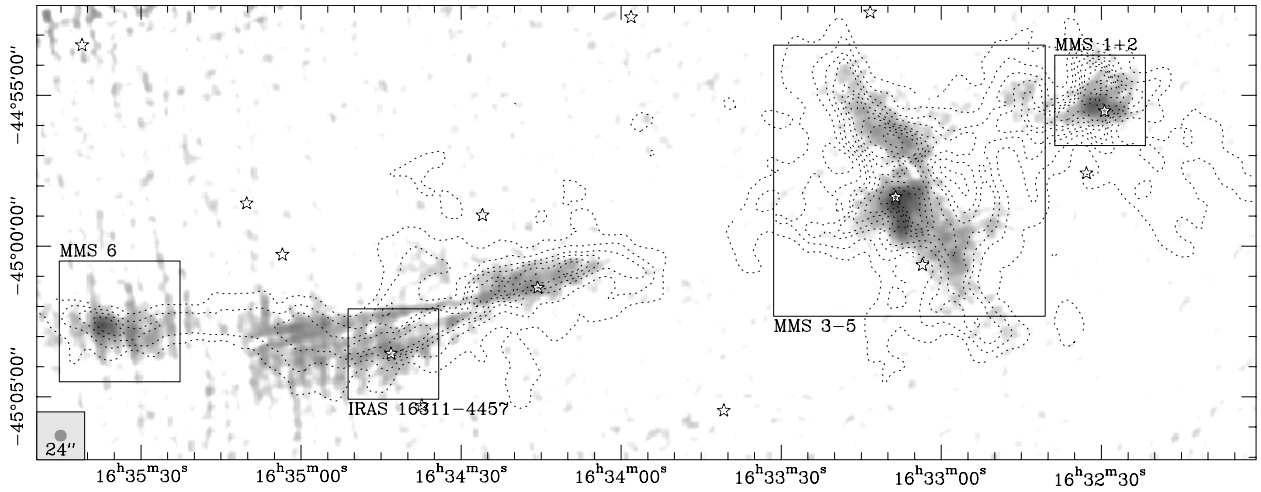

Fig. 2. SIMBA map at $\lambda = 1.2$ mm (grey-scale) superimposed with contours showing the absorption structure in the DSS image smoothed to the resolution of the mm map. The stars represent *IRAS* point-sources. The boxes indicate the cut-outs of the individual sources we show in Sect. 3.2. The coordinates are given in right ascension and declination in J2000.

extinction of more than $A_V = 3.7$ mag. The corresponding values for the eastern region of the mm map are $N(H_2) = 1.3 \times 10^{22}$ cm^{-2} and $A_V = 6.9$ mag.

In cases where the spectral coverage including *2MASS* and *MSX* data is sufficient, we carried out two-component blackbody fits in the IR regime with an additional grey-body component in the submm range. Since the spatial resolution of the *IRAS* data is lower than from any other instrument used in the analysis, we only adopted them as upper limits in the fitting procedure (indicated as downward open triangles in the SEDs). Where available, we also included (sub)mm data from the literature. The ISOPHOT observations of Ábrahám et al. (2004) have spatial resolutions between 43″ and 180″. Therefore, we adopted them as upper limits only (indicated as downward filled triangles in the SEDs). We took the coldest temperature $T_{\rm dust}$ to derive masses from the mm measurement according to Eq. (2) which is valid for optically thin radiation:

$$M = \frac{S_{1.2} D^2}{\eta \kappa_{1.2} B_{1.2}(T_{\rm dust})}. \quad (2)$$

$S_{1.2}$ is the flux density measured at 1.2 mm, D is the distance (700 pc), η is the gas-to-dust ratio (140), and $\kappa_{1.2}$ is the corresponding dust mass absorption coefficient which we assume as 0.2 cm^2 g^{-1}, typical of protostellar matter with coatings (Krügel & Siebenmorgen 1994). Finally, $B_{1.2}(T_{\rm dust})$ is the value of the Planck-function for $T_{\rm dust}$ at 1.2 mm. Altogether, the mass estimate can deviate from the real value by a factor of 10. This uncertainty is dominated by the knowledge of κ. All the other parameters combined introduce an inaccuracy of a factor of 1.5 only.

Integrating under the fitting function yields the total luminosity $L_{\rm tot}$ with an accuracy of 25%. Using $L_{\rm tot}$ as a measure of the bolometric luminosity $L_{\rm bol}$, we can apply the Class 0 criterion for the candidate protostars (André et al. 1993). Here, the submm luminosity $L_{\rm smm}$ is defined as the luminosity beyond $\lambda = 350$ μm while the ratio $L_{\rm bol}/L_{\rm smm}$ determines the evolutionary stage. Sources with ratios < 200 are classified as Class 0 objects. The physical explanation for this threshold is that most of the protostellar material is still in the circumstellar envelope.

Table 1. Positions and source correlations of the compact millimetre sources. The CO and CS peaks refer to Moreira et al. (2000). The positions are determined from the mm map.

Source	α(J2000)	δ(J2000)	association
MMS 1	$16^h32^m27\overset{s}{.}3$	–44°55′29″	Re 13 SM
MMS 2	$16^h32^m31\overset{s}{.}3$	–44°55′21″	V346 Nor
MMS 3	$16^h33^m04\overset{s}{.}8$	–44°58′19″	^{12}CS peak
MMS 4	$16^h33^m07\overset{s}{.}9$	–44°58′34″	^{13}CO peak
MMS 5	$16^h33^m07\overset{s}{.}2$	–44°59′24″	^{12}CO peak
MMS 6	$16^h35^m36\overset{s}{.}8$	–45°02′48″	

3.2. Millimetre sources

Besides the extended emission, the SIMBA map shows 6 compact millimetre sources. Their locations and intensities are listed in Tables 1 and 2.

3.2.1. MMS 1

Figure 3 provides a closer look at the compact mm sources MMS 1 and 2. MMS 1 roughly coincides with the reflection nebula Reipurth 13 (Re 13) (Reipurth 1981). It is illuminated by a deeply embedded stellar source that powers the Herbig-Haro flow HH 56 (Reipurth et al. 1997). A previous single beam measurement (Reipurth et al. 1993) gave a value of $S_{1.3} = 102 \pm 7$ mJy. A consistent result was published by Sandell & Weintraub (2001) who also present submillimetre measurements at 450 μm and 850 μm. Our data corroborates their claim that the (sub)mm source labelled Reipurth 13 SM does not match the optical and infrared source position. MMS 1 and Re 13 SM much better agree with an *MSX* source, only 5″ away from the nominal position of the mm source. According to the *2MASS* database, there are two NIR sources in its

Table 2. Photometry and properties of the compact millimetre sources. They all appear point-like in the *MSX* images. The sizes of the fitted Gaussians inferred at 1.2 mm are listed as well.

	MSX				SIMBA					
	Photometry				Gaussian fit		Photometry			
Source	S_A [mJy]	S_C [mJy]	S_D [mJy]	S_E [mJy]	major axis	axis ratio	$S_{1.2}$ [mJy]	$L_{\rm tot}$ [$L_\odot$]	$L_{\rm tot}/L_{\rm smm}$	$M_{\rm gas}$ [$M_\odot$]
MMS 1	648 ± 11	873 ± 56	1196 ± 58	1709 ± 98	35.″5	0.67	97 ± 25	31	207	0.3
MMS 2	5675 ± 41	8921 ± 125	10348 ± 97	13137 ± 216	44.″5	0.72	382 ± 37	120	632	0.5
MMS 3	<15	<140	<160	1136 ± 90	69.″9	0.69	11300 ± 63	53	13	45.1
MMS 4	567 ± 7	813 ± 46	1419 ± 53	2415 ± 113						
MMS 5	<15	<140	<160	<270	42.″4	0.80	417 ± 40	–	–	2.4
MMS 6	absorption	<195	194 ± 24 (?)	<430	43.″6	0.80	452 ± 43	–	–	2.7

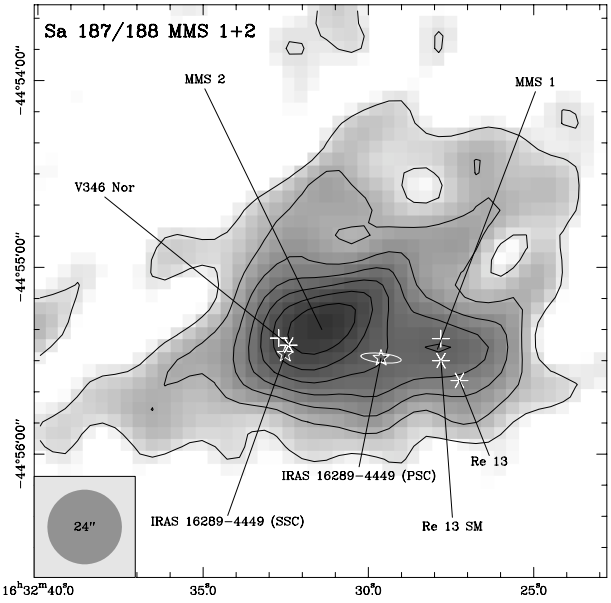

Fig. 3. SIMBA map of MMS 1 and 2. The contours denote flux levels from 3σ rms to the peak flux in steps of 3σ. Individual objects are labelled. The crosses (+) locate the positions of *MSX* point sources. The coordinates are given in J2000. The size of the telescope beam is indicated in the lower left corner.

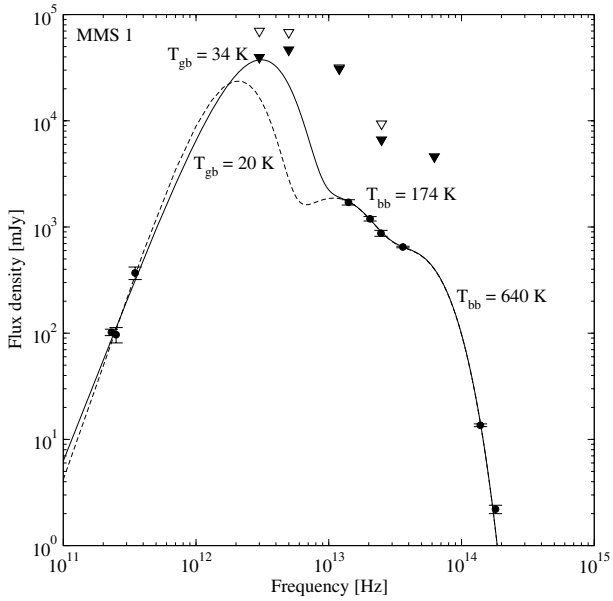

Fig. 4. Spectral energy distribution of MMS 1. The data include *2MASS*, *MSX*, the SCUBA measurement of Sandell & Weintraub (2001), the mm observations of Reipurth et al. (1993) as well as our own SIMBA photometry. The *IRAS* data (▽) and ISOPHOT observations of Ábrahám et al. (2004) (▼) must be attributed to more than only one source because of the large beams. Therefore, they are added as upper limits only.

immediate vicinity separated by only 1.″5. One of them is detected in K_S, the other one in H only. Both sources satisfy the Class I criterion for YSOs when including the *MSX* data. Prusti et al. (1993) report on NIR photometry of Re 13 and V346 Nor, but their observing technique made use of a diaphragm with a size of 12″ which obviously produced unreliable values because of source confusion.

Including the data of the neighbouring *IRAS* PSC source IRAS 16289-4449, a three-component fit (1 grey-body, 2 black-bodies, see Fig. 4) to the data demonstrates that both *2MASS* sources achieve the same result, so they cannot be distinguished from each other by their properties. We get colour temperatures of 640 K for the hot, 174 K for the warm and 34 K for the cold dust component. The grey-body has a submm emissivity index of $\beta = 1.4$. We derive $L_{\rm tot} = 31\ L_\odot$ and $L_{\rm smm} = 0.15\ L_\odot$ clearly exceeding the threshold for the Class 0 criterion. Therefore, MMS 1 seems to be an embedded moderately evolved PMS star. This characterisation is supported by the fact that we derive a total gas mass of 0.3 $M_\odot$ which is typical for a massive circumstellar disc.

Since the spatial resolution of *IRAS* was much poorer than achieved in our data, the fluxes from the database probably suffer from contamination from the surrounding material. The same argument holds for the ISOPHOT measurements of Ábrahám et al. (2004). For this reason, it might be more realistic to use them as upper limits for MMS 1 only. This does not affect the NIR to MIR range, but fitting the (sub)mm data becomes unreliable. Assuming a dust temperature of 20 K, the new values are $\beta = 2.0$, $L_{\rm tot} = 18\ L_\odot$ and $M_{\rm gas} = 0.6\ M_\odot$.

3.2.2. MMS 2

MMS 2 coincides with the FU Ori star V346 Nor driving the HH 57 flow. It underwent a large outburst in 1983 and continued to show brightness variations in the following years (Graham & Frogel 1985). Ábrahám et al. (2004) even report on a recent increase of the NIR flux. The variations are possibly

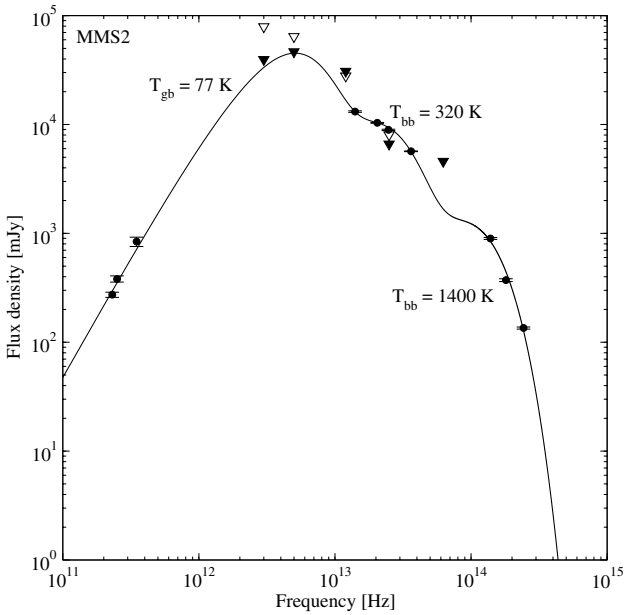

Fig. 5. Spectral energy distribution of MMS 2.

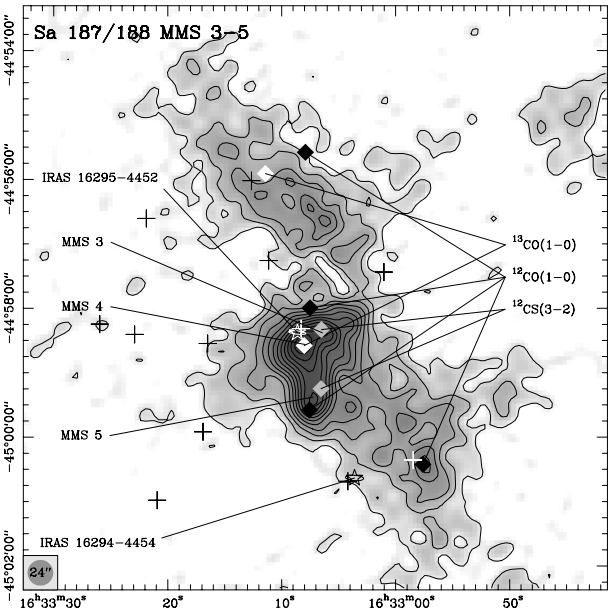

Fig. 6. SIMBA map of MMS 3 to 5. The peaks of molecular line emission in ^{12}CO(1–0), ^{13}CO(1–0) and ^{12}CS(3–2) are taken from Moreira et al. (2000). Additional labelling and contours as in Fig. 3.

caused by an expanding shell or circumstellar disc that contain dense material re-processing the stellar light. The NIR colours as derived from the *2MASS* archive are $(J - H) = 1.58$ and $(H - K_S) = 1.42$ suggesting that V346 Nor exhibits a large NIR colour excess corroborating the existence of circumstellar material. Its spectral index (Lada 1987) between K_S and the *MSX* *E*-band is 0.3, hence similar to a Class I object.

Reipurth et al. (1993) found a millimetre flux of $S_{1.3} = 273 \pm 15$ mJy. A similar value was found by Sandell & Weintraub (2001) who also list values at 450 μm and 850 μm. The *IRAS* source IRAS 16289-4449 has been assigned to it, but one has to distinguish between the entry in the point-source catalogue (PSC) and the serendipity survey catalogue (SSC) which both use the same labelling of the IR sources. While the position of the PSC object lies between MMS 1 and MMS 2 and its flux is probably affected by both, the SSC object is located close to MMS 2 and is therefore most likely identical to V346 Nor. The photometry of the *MSX* source coinciding with its position also matches the values of the *IRAS* SSC source. The mm photometry is strongly affected by the surrounding faint emission leading to an uncertain value for the compact component. However, significant contamination by free-free emission can be excluded, as Curiel et al. (1989) did not find any radio continuum source coinciding with V346 Nor.

All these data can be best fitted with a 2-component blackbody yielding colour temperatures of 320 K and 1400 K combined with an additional grey-body fit (Fig. 5). We obtain 77 K for the cool dust component along with an emissivity index of $\beta = 0.3$. These values lead to a total gas mass of 0.5 $M_\odot$ and $L_{tot} = 120\ L_\odot$. This is in good agreement with the values derived by Sandell & Weintraub (2001). However, we think this is only a coincidence, because these authors adopted dust properties quite different to what we used. They also assumed a typical dust temperature of 50 K, while we estimate it from the measurements. MMS 2 does not satisfy the Class 0 criterion.

3.2.3. MMS 3 to 5

A detailed view of the compact sources MMS 3 to 5 is available in Fig. 6. This region was also covered by the molecular line observations of Moreira et al. (2000). The locations of the peaks of the line emission are indicated. MMS 3 coincides with a ^{12}CS(3–2) peak, MMS 4 with a maximum in ^{13}CO(1–0) and MMS 5 matches a ^{12}CO(1–0) peak. Further maxima are embedded in the millimetre continuum emission that extends to the North and South.

MMS 4 roughly coincides with IRAS 16295-4452 which is listed with different coordinates in the PSC and the SSC. While the SSC source has only low upper flux limits in almost every *IRAS* filter – which contradicts our *MSX* photometry – the PSC source shows compatible intensities. MMS 4 can also be associated with both an NIR and an MIR source. However, they are about 10″ away from the mm peak. The NIR colours of $(J - H) = 2.27$ and $(H - K_S) = 1.64$ suggest a visual extinction $A_V \approx 20$ mag. The spectral index between *2MASS* K_S and the *MSX* *E*-band of 1.4 corroborates its nature of a YSO. However, there is another *2MASS* source about 20″ south of this object whose position much better matches the *IRAS* source. It was not detected in *J*, hence its NIR colours are $(J - H) > 2.42$ and $(H - K_S) = 2.82$. The IR colours were already discussed by Moreira et al. (2000) who classified this object as a "bona fide Class I protostar"; we derive a spectral index of 1.4 corroborating this assessment. MMS 3 is only a faint source in the *MSX* *E*-band and has no NIR counterpart in the *2MASS* database.

Unfortunately, MMS 3 and MMS 4 cannot be analysed individually. Although they are clearly separated in the *MSX* images, the mm emission is complex and contaminated by an inhomogeneous background. Therefore, we measured the combined mm flux density of both sources as demonstrated in Table 2. The SED fitting procedure did not converge to a

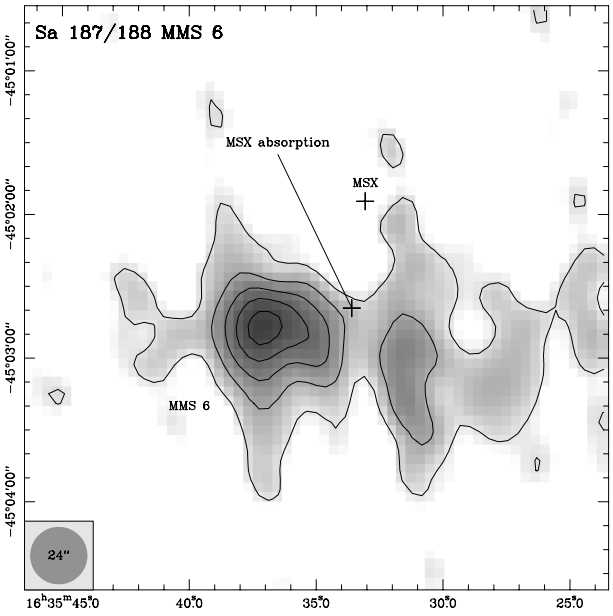

Fig. 7. SIMBA map of MMS 6. See Fig. 3 for labelling and contours.

reliable solution. The formal colour temperature derived from the 1.2 mm and the *IRAS* 100 μm data is 27 K. We used this value to estimate a total gas mass of 45 $M_\odot$ which indicates a mean column density of $N(H_2) = 9.4 \times 10^{22}$ cm^{-2} inside the integration region. If we modify the core mass determined by Moreira et al. (2000) by shifting the cloud to a distance of 700 pc, it amounts to 48 $M_\odot$. Since we could not derive the luminosity from the SED fitting function, we used the data points themselves. The corresponding result is $L_{\rm tot} = 53\ L_\odot$.

MMS 5 has a NIR counterpart, but no emission at MIR wavelengths as evident from the *MSX* data. The reason for this discrepancy is possibly a pure coincidence of sources. The *2MASS* NIR magnitudes can be fitted with a simple black-body of $T = 4740$ K steeply declining into the MIR regime. The NIR colours of $(J - H) = 0.33$ and $(H - K_S) = 0.12$ suggest a visual extinction of only $A_V = 3$. These values are consistent with a MS star of spectral type A at a distance of 400 pc, i.e. in front of the cloud. The de-reddened black-body has a temperature in the range of $T = 10\,000$ K, corroborating this estimate. Therefore, we have to rely on a guess for the dust temperature of the mm source which we assume is $T_{\rm dust} = 20$ K. The resulting gas mass of MMS 5 is $M = 2.4\ M_\odot$. This corresponds to a column density of $N(H_2) = 1.2 \times 10^{22}$ cm^{-2}.

3.2.4. MMS 6

Figure 7 is a close-up view of MMS 6. The residual noise amounts to 11.4 mJy/beam and is higher than in other parts of the map due to a poorer coverage of this region. However, the detection of MMS 6 is beyond doubt (15σ for the peak). No other counterpart could be found in the literature. Interestingly, the *MSX* data provide an IR absorption feature in the *A*-band and a possible weak detection in the *D*-band, suggesting a very cold core or a protostar.

Integrating the "negative" emission, we get an absorption strength in the *A*-band of 60 mJy corresponding to an optical depth of $\tau_A = 4.4$ using the method of Siebenmorgen & Krügel (2000). This is equivalent to a visual extinction of $A_V = 145$ mag. Using a ratio of total to selective extinction of $R = 3.09$ and the conversion factor of Bohlin et al. (1978), this leads to a column density of $N(H_2) = 2.7 \times 10^{24}$ cm^{-2}. However, these values are uncertain, since we interpolated the extinction law at 8.28 μm from Rieke & Lebofsky (1985) without being able to correct for the filter transmission. Furthermore, it is likely that the sensitivity is not sufficient to detect the background radiation that penetrates the densest part of the source which is necessary to derive accurate estimates for the optical depth. The derived values are therefore only lower limits. Nevertheless, it seems that MMS 6 is the youngest object in the list of mm sources.

Just as for MMS 5, we assume a dust temperature of $T_{\rm dust} = 20$ K and derive a mass of $M = 2.7\ M_\odot$ for MMS 6. If equally distributed across the integration area, this corresponds to a column density of $N(H_2) = 1.2 \times 10^{22}$ cm^{-2} being 225 times lower than the estimate from the IR photometry. However, at a column density of $N(H_2) = 1.25 \times 10^{24}$ cm^{-2} even dust emission at $\lambda = 1.2$ mm becomes optically thick. For such conditions, Eq. (2) no longer applies, and the results are too low. Therefore, our mass estimate is only a lower limit for the true gas mass of MMS 6.

Furthermore, the protostar itself is not resolved so that the bulk of the source mass is concentrated within a smaller volume than covered by our integration area. Therefore, the intrinsic column density is higher than our estimate from the mm data.

3.3. Infrared sources

Although contained within the contours of the millimetre emission, the weak *IRAS* sources IRAS 16306-4455 and IRAS 16311-4457 do not stand out as compact mm sources. Reipurth et al. (1997) reported associated molecular outflows detected in CO which we can identify in our mm map (see Fig. 8).

IRAS 16306-4455 (not shown) was only detected in the 25 μm and 60 μm *IRAS* bands. Our analysis of the *MSX* data yields flux densities of 47 ± 4 mJy in *A*, <105 mJy in *C*, <100 mJy in *D* and <240 mJy in *E*. The photometry of the mm peak coinciding with the IR source position results in a flux density of 55 ± 5 mJy. The *2MASS* database lists a source with $K_S = 14.66$ mag. By combining all these data, we determine a luminosity of $L_{\rm tot} = 4.2\ L_\odot$ and a total mass of $M_{\rm tot} = 0.1\ M_\odot$.

IRAS 16311-4457 is a weak *IRAS* source which was only detected in the 25 μm band. The *MSX* data provide flux densities of 141 ± 6 mJy in *A*, 447 ± 49 mJy in *C*, <110 mJy in *D* and <315 mJy in *E*. The two strongest mm peaks in that area coincide with the outflow detected by Reipurth et al. (1997) having a combined flux density of 230 ± 36 mJy at $\lambda = 1.2$ mm. Including the *JHKL* photometry of Reipurth et al. (1997), we derive a luminosity of $L_{\rm tot} = 9.4\ L_\odot$ and a total mass of $M_{\rm tot} = 0.8\ M_\odot$.

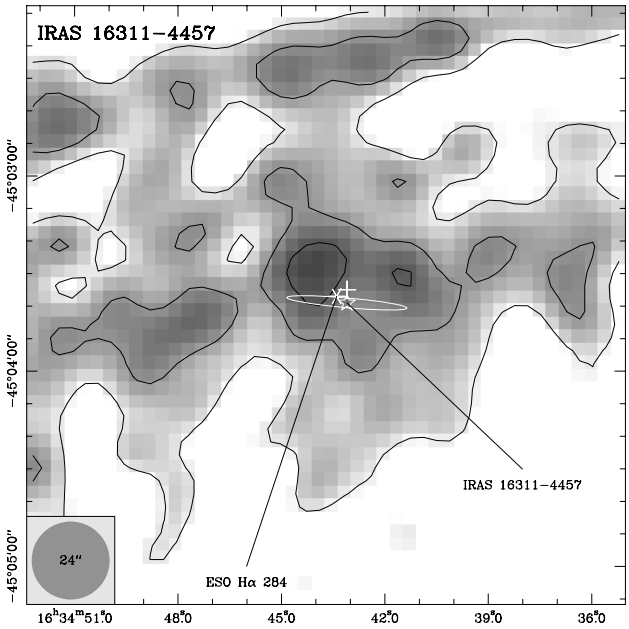

Fig. 8. SIMBA map of the area around IRAS 16311-4457 indicated with its positional error ellipse. The two strongest peaks coincide with the location of the outflow lobes (Reipurth et al. 1997). Labelling and contours as in Fig. 3.

4. Discussion

4.1. The protostellar content of Sa 187/188

Our data corroborate previous results that a young stellar population resides in Sa 187/188. There are already moderately evolved pre-main sequence stars like V346 Nor. Our inspection of the *2MASS* database reveals three additional NIR colour excess sources that mostly reside in the western part of Sa 187/188. This number may increase, however, because many *2MASS* sources within the cloud boundaries have $H - K_S$ colours suggestive of embedded members; unfortunately they were not detected in the J-band.

The detection of MMS 6 demonstrates that even younger pre-stellar phases co-exist, and star formation is still very active. As explained in Sect. 3.2.4, this mm source is IR-dark and therefore a probable pre-protostellar core.

Although the total number of detected YSOs is still low, there seems to be an age gradient of stellar sources indicating a star formation history proceeding from the East to the West. The youngest object is clearly MMS 6 located at the eastern tip of the filament. Farther to the West, there are the *IRAS* sources IRAS 16306-4455 and IRAS 16311-4457 exhibiting strong molecular outflows (see Sect. 3.3). They are weak at NIR and MIR wavelengths. Even farther to the West, there is the molecular core of MMS 3-5. Table 2 lists a ratio of $L_{\rm tot}/L_{\rm smm} = 13$ for MMS 3 and 4 strongly suggesting a protostellar nature, i.e. Class 0. Finally, there is the most evolved, well studied region around MMS 1 and 2 including V386 Nor. A similar trend of an age sequence along a filamentary cloud was found for OMC 1-3 in Orion A (Nielbock et al. 2003).

4.2. The star formation history of Sa 187/188

Filamentary dark clouds (FDC) are an interesting sub-class of star-forming molecular clouds, as they seem to contradict the classical paradigm of a spherical collapse accompanied by fragmentation. The ISM is confined to a narrow ridge of dust and gas populated with embedded young stellar objects (YSO). However, they often seem to foster the development of dark globules (Schneider & Elmegreen 1979; Leung et al. 1982) by collapse of single cloud fragments. There are well known examples of FDCs like the Orion Molecular Cloud (OMC) (Bally et al. 1987), the R Corona Australis Cloud (R CrA) (Graham & Phillips 1987; Chini et al. 2003), the Lupus Cloud Complex (Andreazza & Vilas-Boas 1996) and the Ophiuchus Cloud Complex (de Geus et al. 1990).

The formation process of FDCs is not well understood. External triggers supporting the formation of filamentary cloud structures could be provided by stellar winds that build up an external pressure which sweeps up the ISM (Schneider & Elmegreen 1979). Expanding super-bubbles interacting with the ISM could be another explanation (Chini et al. 1997; Stegeman 2002). Stellar clusters rather than single stars are thought to be their driving force, in which high-mass stars (O-B) are needed to provide such winds. Examples in low-mass star-forming regions are therefore difficult to explain with externally driven influences.

Hartmann (2002) favours a scenario in which large-scale flows in the ISM lead to the formation of sheetlike structures that eventually collapse under self-gravitation and possibly form filamentary star-forming clouds. Burkert & Hartmann (2004) enhanced this picture by adopting sheets with finite boundaries.

Another concept includes the perturbation of magnetic fields that align the neutral ISM parallel to the field lines and confine it to a narrow ridge (Nagai et al. 1998). Recent polarisation studies of OMC 2/3 corroborate the orientation of the dense ISM being aligned with the local magnetic field (Matthews & Wilson 2000).

In the case of Sa 187/188, we believe that the cloud could have undergone an evolution outlined by Fig. 11 of Burkert & Hartmann (2004): there the FDC is a result of a collapsing elliptical sheet with an initial density gradient along the major axis. As a consequence, the collapse commences only at one end and proceeds to the other end inducing star formation events along the resulting filament which depend on the speed of the propagating collapse. If we take Eq. (9) from Burkert & Hartmann (2004) and modify it by replacing the cloud radius R and the mass surface density Σ with the cloud diameter D and the column density N, respectively, we can estimate a typical time scale for this event:

$$t_C = \sqrt{\frac{D}{\pi G \mu N(\mathrm{H_2})}}. \quad (3)$$

We find a collapse time scale of the order of 2×10^6 years which appears to be consistent with the age gradient of pre-stellar sources within Sa 187/188.

From Eqs. (4) and (5) of Hartmann (2002) we can determine the critical Jeans length λ_c and the critical mass for a

fragment M_c inside a filament. For Sa 187/188, we find λ_c = 0.2 pc, i.e. 1′ at a distance of 700 pc being of the order of the filament diameter. The corresponding critical mass amounts to $M_c = 3\ M_\odot$. Note that MMS 6, the youngest object detected in Sa 187/188, exhibits a mass of $M_{gas} = 2.7\ M_\odot$. Considering these results we speculate that Sa 187/188 might have had a filament formation history as proposed by Burkert & Hartmann (2004).

5. Conclusions

By combining our 1.2 mm continuum data with IR measurements from *IRAS*, *MSX* and *2MASS*, we investigated the stellar content in Sandqvist 187/188, also known as the Norma cloud. We studied the properties of the extended mm emission and six compact mm sources. In particular we obtained the following results:

1. The extended mm emission is well aligned with the optical dark cloud. The achieved sensitivity allows us to trace the cloud ISM down to a column density of $N(H_2) = 7.0 \times 10^{21}$ cm^{-2} being equivalent to a visual extinction of A_V = 3.7 mag. We determine a mean column density for the Sa 187/188 cloud of $N(H_2) = 1.4 \times 10^{22}$ cm^{-2} which corresponds to a visual extinction of $A_V = 7.6$ mag. We find a total mass of 340 $M_\odot$.
2. We detect six compact millimetre continuum sources with gas masses between 0.3 and 2.7 $M_\odot$. MMS 3 and 4 possess a combined gas mass of 45 $M_\odot$ possibly including some of the background material as well.
3. The few sources seem to indicate an age gradient along the filament. The most evolved objects (i.e. V346 Nor) populate the western region of the cloud. The Class 0 object MMS 4 along with the molecular cores are located more to the East followed by the cold and dense MMS 6 at the most eastern end of Sa 188. A similar trend was found in the FDC of OMC 1 to 3 (Nielbock et al. 2003).
4. The distance of the complex is found to be at least 440 ± 50 pc and thus excludes previous lower distance estimates.

Acknowledgements. The authors wish to thank B. Reipurth and K. Kämpgen for useful comments.
This research has made use of the SIMBAD and VizieR databases, operated at CDS, Strasbourg, France and the NASA/IPAC Infrared Science Archive, which is operated by the Jet Propulsion Laboratory, California Institute of Technology, under contract with the National Aeronautics and Space Administration. This publication also makes use of data products from the Two Micron All Sky Survey, which is a joint project of the University of Massachusetts and the Infrared Processing and Analysis Center/California Institute of Technology, funded by the National Aeronautics and Space Administration and the National Science Foundation. Furthermore, this project benefitted from data of the Midcourse Space Experiment. Processing of the data was funded by the Ballistic Missile Defense Organization with additional support from the NASA Office of Space Science.

References

Ábrahám, P., Kóspál, Á., Csizmadia, S., et al. 2004, A&A, 428, 89
Alvarez, H., Bronfman, L., Cohen, R., et al. 1986, ApJ, 300, 756
André, P., Ward-Thompson, D., & Barsony, M. 1993, ApJ, 406, 122
Andreazza, C. M., & Vilas-Boas, J. W. S. 1996, A&AS, 116, 21
Bally, J., Stark, A. A., Wilson, R. W., & Langer, W. D. 1987, ApJ, 312, L45
Bohlin, R. C., Savage, B. D., & Drake, J. F. 1978, ApJ, 224, 132
Bourke, T. L., Hyland, A. R., & Robinson, G. 1995, MNRAS, 276, 1052
Burkert, A., & Hartmann, L. 2004, ApJ, 616, 288
Cannon, A. J., & Mayall, M. W. 1949, Annals of Harvard College Observatory, 112, 221
Carpenter, J. M. 2001, AJ, 121, 2851
Chini, R., Kämpgen, K., Reipurth, B., et al. 2003, A&A, 409, 235
Chini, R., Reipurth, B., Ward-Thompson, D., et al. 1997, ApJ, 474, L135
Cohen, M., Schwartz, R. D., Harvey, P. M., & Wilking, B. A. 1984, ApJ, 281, 250
Curiel, S., Rodriguez, L. F., Canto, J., & Torrelles, J. M. 1989, Rev. Mex. Astron. Astrofis., 17, 137
de Geus, E. J., Bronfman, L., & Thaddeus, P. 1990, A&A, 231, 137
Egan, M. P., Price, S. D., Moshir, M., et al. 1999, The Midcourse Space Experiment Point Source Catalog Version 1.2 Explanatory Guide, Tech. Rep. AFRL-VS-TR-1999-1522, Air Force Research Laboratory
Graham, J. A., & Frogel, J. A. 1985, ApJ, 289, 331
Graham, J. A., & Phillips, A. C. 1987, PASP, 99, 91
Gregorio Hetem, J. C., Sanzovo, G. C., & Lépine, J. R. D. 1988, A&AS, 76, 347
Hartmann, L. 2002, ApJ, 578, 914
Krügel, E., & Siebenmorgen, R. 1994, A&A, 288, 929
Lada, C. J. 1987, in Star Forming Regions, ed. M. Peimbert, & J. Jugaku (Dordrecht: D. Reidel Publishing Co.), IAU Symp., 115, 1
Leung, C. M., Kutner, M. L., & Mead, K. N. 1982, ApJ, 262, 583
Matthews, B. C., & Wilson, C. D. 2000, ApJ, 531, 868
Moreira, M. C., Jessop, N. E., Santos, C. A., & Yun, J. L. 2000, AJ, 119, 2960
Nagai, T., Inutsuka, S., & Miyama, S. M. 1998, ApJ, 506, 306
Nesterov, V. V., Kuzmin, A. V., Ashimbaeva, N. T., et al. 1995, A&AS, 110, 367
Nielbock, M., Chini, R., & Müller, S. A. H. 2003, A&A, 408, 245
Nyman, L.-Å., Lerner, M., Nielbock, M., et al. 2001, The Messenger, 106, 40
Prusti, T., Bontekoe, T. R., Chiar, J. E., Kester, D. J. M., & Whittet, D. C. B. 1993, A&A, 279, 163
Reichertz, L. A., Weferling, B., Esch, W., Kreysa, E., & Sievers, A. 2001, A&A, 379, 735
Reipurth, B. 1981, A&AS, 44, 379
Reipurth, B., Chini, R., Krügel, E., Kreysa, E., & Sievers, A. 1993, A&A, 273, 221
Reipurth, B., Olberg, M., Gredel, R., & Booth, R. S. 1997, A&A, 327, 1164
Rieke, G. H., & Lebofsky, M. J. 1985, ApJ, 288, 618
Sandell, G., & Weintraub, D. A. 2001, ApJS, 134, 115
Sandqvist, Å. 1977, A&A, 57, 467
Schneider, S., & Elmegreen, B. G. 1979, A&AS, 41, 87
SEST. 2003, SIMBA Observers Manual
Siebenmorgen, R., & Krügel, E. 2000, A&A, 364, 625
Stegeman, I. M. 2002, in Interacting Winds from Massive Stars, ed. A. F. J. Moffat, & N. St-Louis (San Francisco: The Astronomical Society of the Pacific), ASP Conf. Ser., 260, 47

Online Material

Appendix A: Coinciding infrared sources

Table A.1. Positions of infrared sources coinciding with the compact millimetre sources as they are listed in the databases. The positions for MMS 3 and the *MSX* absorption feature of MMS 6 were derived manually from the images.

	2MASS		*MSX*	
Source	α(J2000)	δ(J2000)	α(J2000)	δ(J2000)
MMS 1	$16^h32^m27\overset{s}{.}2$	–44°55′30″	$16^h32^m27\overset{s}{.}2$	–44°55′30″
	$16^h32^m27\overset{s}{.}2$	–44°55′32″		
MMS 2	$16^h32^m32\overset{s}{.}2$	–44°55′31″	$16^h32^m32\overset{s}{.}2$	–44°55′30″
MMS 3	–		$16^h33^m06\overset{s}{.}2$	–44°58′07″
MMS 4	$16^h33^m07\overset{s}{.}7$	–44°58′25″	$16^h33^m07\overset{s}{.}8$	–44°58′13″
MMS 5	–		–	
MMS 6	–		$16^h35^m33\overset{s}{.}4$	–45°02′40″

Appendix B: The distance to Sa 187/188

The distance of Sa 187/188 is not well constrained. A first crude estimate of 200 pc was given by Cohen et al. (1984), who put Sa 187/188 in relation to clouds that extend into the Lupus region. On the other hand, Graham & Frogel (1985) determined a value of 700 pc ± 50% by analysing the optical photometry of foreground stars and assumed they are main-sequence (MS) stars of spectral type later than G. In addition, they claim an upper limit of 1100 pc based on the CO measurements of Alvarez et al. (1986) combined with a galactic rotation model. Gregorio Hetem et al. (1988) favour a value of 150 pc from the analysis of the absolute magnitudes of *IRAS* sources without specifying their procedure in detail.

We tried an approach similar to Graham & Frogel (1985) based on infrared data from the *2MASS* project whose quality is superior to the data they used in their analysis. For accuracy, we only picked detections with photometric errors <0.1 mag. HD 328329 and HD 328406 are A2 and F0 MS stars (Cannon & Mayall 1949; Nesterov et al. 1995), respectively, both located in front of the dark cloud coinciding with bright *2MASS* sources. Their coordinates are α(J2000) = $16^h32^m32\overset{s}{.}66$, δ(J2000) = −44°56′39″.1 for HD 328329 and α(J2000) = $16^h35^m12\overset{s}{.}43$, δ(J2000) = −45°03′36″.3 for HD 328406.

Using the *2MASS* JHK_S data we derive a foreground extinction of 1.5 mag and a distance of 490 pc for HD 328329; the corresponding values for HD 328406 are 0.8 mag and 390 pc, respectively. The extinction increment towards HD 328406 is only 0.2 mag per 100 pc, while it rises to 0.7 mag per 100 pc towards HD 328329. This increase seems to indicate that the edge of the cloud is located at a distance somewhere between 390 and 490 pc. However, we cannot make any statement as to the depth of the cloud, preventing any further constraints on the cloud distance. Additional observations such as *UBV* photometry or spectral classification of reddened stars are needed for that. We therefore take 440 ± 50 pc as a good lower limit for Sa 187/188 and exclude previous lower distance estimates.

Table C.1. Extinction law in the JHK_S *2MASS* colour system as derived from Rieke & Lebofsky (1985).

λ	$\frac{E_{\lambda-V}}{E_{B-V}}$	$\frac{A_\lambda}{A_V}$
J	–2.25	0.271
H	–2.60	0.157
K_S	–2.76	0.106

Appendix C: The extinction law in the *2MASS* colour system

The *2MASS* colour system significantly deviates from the standard Johnson-Koornneef system which Rieke & Lebofsky (1985) used to determine the near-infrared (NIR) extinction law. The main difference is the use of the Johnson *K* filter and the *2MASS* K_S filter. Hence, in order to be able to draw conclusions from the NIR characteristics of the stars in Sa 187/188, as done in Appendix B, we transformed the parameters of the extinction law into the *2MASS* system following the transformation equations listed in Carpenter (2001)[3]. The result is shown in Table C.1.

Although these numbers do not seem to differ very much from the original extinction law, their impact on the reddening slopes in the colour–colour and colour–magnitude diagrams is severe (see Eqs. (C.1) and (C.2)).

$$\left.\frac{E_{J-H}}{E_{H-K}}\right|_{\text{Johnson}} = 1.7 \qquad \left.\frac{E_{J-H}}{E_{H-K_S}}\right|_{2MASS} = 2.2 \qquad \text{(C.1)}$$

$$\left.\frac{A_J}{E_{J-H}}\right|_{\text{Johnson}} = 2.6 \qquad \left.\frac{A_J}{E_{J-H}}\right|_{2MASS} = 2.4. \qquad \text{(C.2)}$$

[3] We used the updated values from the *2MASS* manual (`http://www.ipac.caltech.edu/2mass/releases/allsky/doc/sec6_4b.html`).